Liquid Crystals
Publication details, including instructions for authors and subscription information:
http://www.informaworld.com/smpp/title~content=t713926090

Magnetic and electric field induced bistability in nematics and cholesterics

U. D. Kini[a]
[a] Raman Research Institute, Bangalore, India

To cite this Article Kini, U. D.(1991) 'Magnetic and electric field induced bistability in nematics and cholesterics', Liquid Crystals, 10: 5, 597 — 621
To link to this Article: DOI: 10.1080/02678299108241729
URL: http://dx.doi.org/10.1080/02678299108241729

LIQUID CRYSTALS, 1991, VOL. 10, NO. 5, 597–621

Magnetic and electric field induced bistability in nematics and cholesterics

by U. D. KINI
Raman Research Institute, Bangalore-560080, India

(*Received 24 September 1990; accepted 13 March 1991*)

Continuum theory is used for setting up the differential equations governing bistable behaviour of the director field (**n**) in nematics having positive diamagnetic susceptibility anisotropy χ_a, the bistability being induced by slowly rotating a magnetic field **H** away from $\mathbf{n}_0$, the initial uniform director orientation. The bistability width w_b is the range of magnetic tilt angle over which two different equilibrium configurations can exist. Under the rigid anchoring hypothesis two simple cases are studied (viz. the splay/bend and twist geometries) in which **n** is described by a single orientational degree of freedom and **H** rotates about an axis which is either normal to or parallel to the sample planes. The splay/bend geometry can be generalized to uniformly tilted $\mathbf{n}_0$ and to non-symmetric director tilt at the boundaries; the twist geometry can be extended to include twisted nematics as well as chiral nematics (or cholesterics having equilibrium pitch of the order of the sample thickness). Bistability should be observable even in situations where a Freedericksz threshold does not exist. The width w_b is found to depend on the geometry, **H** and on $\mathbf{n}_0$ (and also on the equilibrium pitch for the chiral systems). For rigid anchoring, scaling analysis shows that w_b should depend only on the reduced field for given material parameters and tilt of $\mathbf{n}_0$ and suggests the need for experiments using different sample thicknesses. When the director anchoring at the sample planes is weakened, w_b varies sensitively with anchoring strength. When the anchoring is weak enough and **H** strong enough there might occur a discontinuous transition from a deformed state to one in which n is oriented uniformly parallel to **H**. The simple scaling which is valid for rigid anchoring does not hold for weak anchoring. A transition between two distortion states should be accompanied by transient flow in the splay/bend geometry; in the twist case, a transition may occur even without accompanying flow. Scaling analysis indicates that the time of transition between two states might depend on sample thickness. Linear stability analysis shows that **n** has a propensity towards instability near the edges of the bistable region. The governing equations can be extended to the case of **H** rotating at a uniform rate, a situation which is of current experimental interest. An electric field, **E**, acting along the sample planes affects the scaling. The electric field as well as the magnitude of the dielectric anisotropy ε_a (>0) now determine w_b. Flexoelectricity, which appears even as a volume effect for large deformations, may have considerable influence on w_b especially for weak anchoring when **E** is impressed. Magnetic field induced bistability should be observable in more complex configurations in which **n** is described by two orientational degrees of freedom; this suggests generalizations of the rotating field experiments. In this context the case of a $\chi_a < 0$ nematic is briefly studied.

1. Introduction

The continuum theory [1–8] has met with a fair measure of success in explaining various phenomena related to the static and dynamic behaviour of nematics and cholesterics. These materials have generated considerable interest mainly because of the various effects which arise through the interaction between the director orientation

0267-8292/91 $3·00

n and external orienting fields (**E**, **H**) and also because of the coupling between orientation and flow. In particular, the **H** induced Freedericksz effect in ($\chi_a > 0$) nematics has been useful for determining the curvature elastic constants. Above the transition, transient flow effects [9, 10] are induced by a viscous stress which is brought into existence by the time rate of change of **n**. The threshold H_F becomes a characteristic field for the given geometry.

It is well known that **H** acting along $\mathbf{n}_0$ (or $-\mathbf{n}_0$) is a purely stabilizing field for χ_a positive nematics. If **H** is impressed at some angle ψ with $\mathbf{n}_0$ ($0 < \psi < \pi/2$) a monodomain deformation results without threshold. On the other hand with **H** normal to $\mathbf{n}_0$ a distortion occurs only above a threshold and more than one domain of deformation can form separated by domain walls. Thus the following question arises: Suppose we start with **H** acting along $\mathbf{n}_0$ (or $-\mathbf{n}_0$) and rotate **H** in small steps away from $\mathbf{n}_0$ such that the axis of rotation is normal to $\mathbf{n}_0$. How does the distortion change?

In principle, there must occur some transient effect each time **H** is rotated away from its present direction. If the rotation is executed in small steps these effects can be ignored and the problem can be treated from the point of view of statics. This was done by Onnagawa and Miyashita [11] when they addressed a theoretical and experimental investigation. They found that the nature of variation of deformation depends ciritically on the strength H of the field. Using capacitance measurements they showed that when $H < H_F$ the distortion (and hence the capacitance) changes continuously when **H** is rotated from $\mathbf{n}_0$ towards $-\mathbf{n}_0$. When $H > H_F$, however, a discontinuous change can be discerned in the capacitance as the tilt of **H** crosses a certain value; in this case, the capacitance exhibits hysteresis when the direction of rotation of **H** is reversed. The theoretical analysis was extended more rigorously by Motooka and Fukuhara [12] who showed that, in general, there can exist two stable configurations in a sufficiently strong **H** while there is only one stable deformation possible in weaker fields. Recently, Karn and Shen [13] conducted an optical investigation of the bistability of homeotropic anchoring; they also studied the transition from an unstable deformation state to a stable configuration.

The effect of **E** on nematics is more complex [6] as the field inside the sample can get modified by director deformations. In many cases flexoelectricity [14] has to be taken into account (see, for example [15]). Recent work [16] has shown that the **E** induced bend transition in nematics with high positive ε_a can be discontinuous; in such materials even the **H** induced splay transition may turn out to be of first order under the stabilizing action of **E** [17]. Theoretical calculations have shown [18] that the combined effects of **E** acting along the sample plane and **H** impressed along different directions may lead to changes in the distortion which may even depend upon the order in which **H** and **E** are applied.

The work on bistability in [11–13] essentially deals with the splay/bend geometry. There is every reason to believe that similar effects may also be observed in the twist geometry with **n** being again described by a single orientational degree of freedom (angle). Undoubtedly **E** acting along or normal to the sample planes should be able to affect the bistability width w_b. It would also be instructive to find out what happens when the ground state, in the absence of external fields, is not uniformly aligned but homogeneously distorted. For instance, in the splay/bend case we could start with some non-symmetric alignments at the boundary [19]; in the twist configuration one can start with either a twisted or a chiral nematic (of pitch of the order of the sample thickness obtained by dissolving chiral impurities in a nematic [5]). The possible effect that weakening of director anchoring at the boundaries [20, 21] might have on w_b must

not be overlooked. The assumption of finite anchoring energy is more realistic than the rigid anchoring hypothesis and may also have a profound influence on field induced deformations [15, 22–24]. An investigation of the total free energy of the different configurations, especially in the region of bistability, becomes necessary. It should be remembered that transient flow might accompany transitions that occur from an unstable to a stable configuration [9, 10]; this may even be amenable to a description by linear stability analysis. Lastly, the various interesting geometries involving rotating fields come to mind (for instance the Tsvetkov experiment [8]; see also [25–28]). One wonders whether the studies on bistability [11–13] can be regarded as being undertaken at the static limit of some more general dynamical situation.

With the above motivation the mathematical model is developed and the method of solution indicated in § 2. Sections 3 and 4 contain results for the splay/bend and twist configurations in various situations. More complex director profiles have been briefly discussed in § 5. Section 6 concludes the discussion.

2. The mathematical model; method of solution

The simplest situation that can arise is one in which **n** is described by a single angle. This is true in the splay/bend and twist geometries. The sample planes are assumed to be at $z = \pm h$ (sample thickness $= 2h$). The deformation angle is assumed to be a function of z and time (t) in the most general case. For evaluating the total free energy F, $10^{-4}\,\mathrm{m}^2$ of the area of either plate is chosen. It is convenient to separately treat the two geometries.

2.1. *Splay/bend geometry*

The easy axes of director anchoring at the sample planes is assumed to be

$$\mathbf{n}(z = \pm h, t) = (\sin\theta_{\pm}, 0, \cos\theta_{\pm}). \tag{2.1}$$

Under the action of

$$\mathbf{H} = (HS_{\psi}, 0, HC_{\psi}); \quad S_{\psi} = \sin\psi; \quad C_{\psi} = \cos\psi \tag{2.2}$$

n is taken to be

$$\mathbf{n}(z, t) = (S_{\theta}, 0, C_{\theta}); \quad \theta = \theta(z, t) \tag{2.3}$$

and the velocity field

$$\mathbf{v}(z, t) = (v_x, 0, 0); \quad v_x = v_x(z, t). \tag{2.4}$$

The volume free energy density at time t is (except for terms independent of distortion)

$$\left.\begin{aligned} W_{v1} &= [f_1(\theta)\theta^2{}_{,z} - \mu_0\chi_a H^2\cos^2(\psi - \theta)]/2; \\ f_1(\theta) &= K_1 S_{\theta}^2 + K_3 C_{\theta}^2; \quad \theta_{,z} = \partial\theta/\partial z, \end{aligned}\right\} \tag{2.5}$$

where K_1 and K_3 are the splay and bend curvature elastic constants, respectively. The surface free energy density at time t is [20, 21]

$$W_{s1} = [\tfrac{1}{2}B_{\theta+}\sin^2\{\theta(z = +h) - \theta_+\}] + [\tfrac{1}{2}B_{\theta-}\sin^2\{\theta(z = -h) - \theta_-\}] \tag{2.6}$$

where $B_{\theta\pm}$ are the (splay/bend) anchoring strengths at $z=\pm h$, respectively. The torque and force equations become

$$\left.\begin{aligned} &f_1(\theta)\theta_{,zz}+\tfrac{1}{2}(df_1/d\theta)\theta^2{}_{,z}+\tfrac{1}{2}\mu_0\chi_a H^2\sin(2\psi-2\theta)\\ &-\gamma_1\dot{\theta}-g_2(\theta)v_{x,z}-\rho_1\ddot{\theta}=0;\quad g_2(\theta)=\mu_2C_\theta^2-\mu_3S_\theta^2\\ &[g_1(\theta)v_{x,z}+g_2(\theta)\dot{\theta}]_{,z}-\rho\dot{v}_x=0; \end{aligned}\right\} \tag{2.7}$$

$$g_1(\theta)=\mu_1S_\theta^2C_\theta^2+\eta_bS_\theta^2+\eta_CC_\theta^2; \tag{2.8}$$

a superimposed dot denotes the time derivative; the μ_i are Leslie viscosity coefficients; the η values are Miesowicz coefficients [5]; γ_1 is the twist viscosity coefficient; ρ is the density; ρ_1 is the moment of inertia density of the director field (ρ and ρ_1, which correspond to inertial effects, are generally ignored). The no-slip condition on v_x is

$$v_x(z=\pm h,t)=0 \tag{2.9}$$

while the boundary conditions on θ take the form

$$\left.\begin{aligned} &[(\partial W_{v1}/\partial\theta_{,z})\pm\tfrac{1}{2}B_{\theta\pm}\sin(2\theta-2\theta_\pm)](z=\pm h,t)=0;\\ &\partial W_{v1}/\partial\theta_{,z}=f_1(\theta)\theta_{,z}. \end{aligned}\right\} \tag{2.10}$$

If the anchoring is rigid equation (2.10) reduces to

$$\theta(z=\pm h,t)=\theta_\pm. \tag{2.11}$$

The splay and bend geometries can be recovered as special cases of the above equations by putting

$$\theta_\pm=0 \tag{2.12}$$

and

$$\theta_\pm=\pi/2. \tag{2.13}$$

In these cases flow accompanies time rate of change of distortion. If **H** is assumed to be rotated in the xz plane (about the y axis, normal to the xz plane which the director field occupies) with uniform angular frequency Ω

$$\mathbf{H}=(H\sin\Omega t,0,H\cos\Omega t) \tag{2.14}$$

(at the end of every period, starting from $t=0$, **H** is along $+z$), equations (2.7)–(2.11) suffice to describe **n** and **v** with the substitution $\psi=\Omega t$ as long as θ is a single valued function of z.

2.2 *Twist geometry*

H and **n** are assumed to be confined to the xy plane. For dependence of **n** on z and t, only a twist distortion is possible and flow is absent. With the easy axes at the two plates given by

$$\mathbf{n}(z=\pm h,t)=(\sin\phi_\pm,\cos\phi_\pm,0) \tag{2.15}$$

it is possible to consider, in principle, both twisted and chiral nematics. With

$$\mathbf{n}(z,t)=(S_\phi,C_\phi,0);\quad \phi=\phi(z,t);\quad \mathbf{H}=(HS_\psi,HC_\psi,0) \tag{2.16}$$

the volume and surface energy densities at time t become

$$W_{v2}=k_2\phi_{,z}+\tfrac{1}{2}K_2\phi^2{}_{,z}-\tfrac{1}{2}\mu_0\chi_aH^2\cos^2(\psi-\phi);\quad k_2=2\pi K_2/P_0; \tag{2.17}$$

$$W_{s2}=[\tfrac{1}{2}B_{\phi+}\sin^2\{\phi(z=+h)-\phi_+\}]+[\tfrac{1}{2}B_{\phi-}\sin^2\{\phi(z=-h)-\phi_-\}], \quad (2.18)$$

where K_2 is the twist elastic constant; P_0 is the equilibrium pitch of the cholesteric, $B_{\phi\pm}$ are the (twist) anchoring strengths at $z=\pm h$, respectively. The torque equation

$$K_2\phi_{,zz}+\tfrac{1}{2}\mu_0\chi_a H^2\sin(2\psi-2\phi)-\gamma_1\dot{\phi}=0 \quad (2.19)$$

is to be solved with the boundary conditions

$$[k_2+K_2\phi_{,z}+\tfrac{1}{2}B_{\phi\pm}\sin(2\phi-2\phi_\pm)](z=\pm h)=0, \quad (2.20)$$

which reduce, for rigid anchoring, to

$$\phi(z=\pm h)=\phi_\pm. \quad (2.21)$$

For a nematic, $k_2=0$ and the boundary values $\phi_\pm$ must be such that $|\phi_+-\phi_-|<\pi/2$ (to ensure non-polarity of **n**). In the case of rigid anchoring for cholesterics it is assumed that the cholesteric helix retains its equilibrium pitch in the absence of external fields [29]. Then, $k_2=(\phi_+-\phi_-)K_2/2h$. For cholesterics there is really no restriction on $\phi_+-\phi_-$. As in § 2.1, by putting $\psi=\Omega t$, we can regard **H** to be rotating in the xy plane with uniform angular frequency Ω.

2.3. *Method of solution*

The complete dynamical problem is not solved; only the static limit is considered by assuming that **H** is rotated very slowly in small steps. The viscous effects are ignored by equating to zero v_x, θ and ϕ; thus **n** becomes a function of z alone. Equations (2.5)–(2.7), (2.10) and (2.11) are examined for the splay/bend geometry and equations (2.17)–(2.20) for the twist configuration. The director orientation profile conforming to the relevant boundary conditions is conveniently obtained by solving the governing equations numerically using the orthogonal collocation method [30, 31] with the zeros of the 24th order Legendre polynomial as collocation points [32].

It is then straightforward to compute the total free energy by gaussian quadrature [32]. As per the assumptions made about the sample dimensions, F is obtained for the rigid anchoring case by integrating the volume free energy density with respect to z between $z=\pm h$ (effectively the sample volume is taken to be $2h\times10^{-4}\,\mathrm{m}^3$). When the anchoring is weak, we add to this integral the surface free energy density computed at $z=\pm h$.

In some situations **n** is described by a symmetric deformation which is a maximum at the sample centre. This quantity yields a natural measure of the total distortion in the sample. It will be seen in due course that the deformation angle at the centre continues to remain a convenient measure of the deformation even when the director field is non-symmetric. The aim of the next two sections will be to study the distortion and F as functions of the field angle for different cases. The material parameters chosen for the model calculation are:

$$\left.\begin{aligned}(K_1, K_2, K_3)&=(3.5, 2.0, 4.2)\times10^{-12}\,\mathrm{N}\ [33];\\ \chi_a&=10^{-6}\ [16].\end{aligned}\right\} \quad (2.22)$$

A sample thickness of $2h=200\,\mu$m has been employed for all calculations. All angles are measured in radians.

3. Results

3.1. *Uniform tilted orientation; rigid anchoring*

The initial uniform orientation is $\mathbf{n}_0=(S,0,C)$ ($S=\sin\theta_0$; $C=\cos\theta_0$) tilted in the xz plane making an angle θ_0 with the z axis; thus, $\theta_\pm=\theta_0$ from equation (2.11). If $\mathbf{H}=(-HC,0,HS)$ is applied in the xz plane normal to $\mathbf{n}_0$, a homogeneous distortion can occur above the threshold

$$H_F=H_F(\theta_0)=(\pi/2h)[f_1(\theta_0)/\mu_0\chi_a]^{1/2}. \tag{3.1}$$

For $\theta_0=0$ (or $\pi/2$) H_F reduces to the bend (or splay) threshold. $R=H/H_F$ provides a convenient measure of H. As the initial configuration is symmetric so is $\theta(z)$ with the extremum $\theta_m=\theta$ ($z=0$).

Initially, $\mathbf{H}$ is along $\mathbf{n}_0$ and consequently there is no deformation, $\theta_m=\theta_0$ itself and F is a minimum. Now $\mathbf{H}$ is rotated away from $\mathbf{n}_0$ in the xz plane. For each ψ, θ_m and F are determined. Next the same procedure is repeated except that $\mathbf{H}$ is rotated away from $-\mathbf{n}_0$ towards $\mathbf{n}_0$. The plots of θ_m and F as functions of ψ are depicted in figure 1 for different R and θ_0 values. The results are in qualitative agreement with those of [11–13].

When $R\leqq 1$, θ_m varies continuously with ψ with no sign of bistability. For $R=1$ the variation is quite sharp close to $\psi=\theta_0+(\pi/2)$. The variation of F is also smooth except that for $R=1$, F changes rather sharply in the middle region (see figures 1 (*a*) and (*b*); for $R\leq 1$ only $\theta_0=0$ has been represented; all details are qualitatively valid for the other two tilt angles). The possibility of a small jump in θ_m as ψ crosses the middle region cannot be ruled out. This is somewhat difficult to establish numerically as ψ has to be varied in very small steps. When $R>1$, however, two branches of the θ_m and F curves result for a given R (see figures 1 (*c*)–(*f*)) due to discontinuous changes occurring as ψ crosses a critical value ψ_c (for example see figures 1 (*c*) and (*d*) for $\theta_0=0$; $R=1{\cdot}4$: transition from J of branch IJ to P of branch LM when $\psi>1{\cdot}87$ or from M of LM to N of IJ when $\psi<1{\cdot}28$). These two disjoint branches can be regarded as representing two distinct sequences of deformations undergone by $\mathbf{n}$, depending upon the particular way or history of ψ variation. For instance (see figures 1 (*c*) and (*d*)) while the branch IJ is obtained by varying ψ from θ_0 towards $\theta_0+\pi$, LM results when ψ is changed from $\theta_0+\pi$ towards θ_0. The overlapping of the two branches on the ψ line results in the bistability width w_b for given θ_0 and R (for instance, the ψ difference between points M and J in figures 1 (*c*) and (*d*)). For given θ_0, w_b increases with R. For a fixed R, w_b decreases as θ_0 is changed from zero (bend geometry) to $\pi/2$ (splay geometry). Interestingly, the region of bistability spreads out equally on either side of the midpoint of the ψ range.

Calculations for different sample thicknesses but the same θ_0 and R show that w_b is unchanged. This is a consequence of scaling which becomes apparent when equations (2.7) and (2.5) are rewritten for the static case with equation (3.1)

$$\left.\begin{aligned} &J(\theta)\,\theta_{,\xi\xi}+\tfrac{1}{2}(dJ/d\theta)\theta^2{}_{,\xi}+\tfrac{1}{2}R^2\sin(2\psi-2\theta)=0;\\ &J(\theta)=4f_1(\theta)/\pi^2 f_1(\theta_0);\quad \xi=z/h; \end{aligned}\right\} \tag{3.2}$$

$$[4h^2/\pi^2 f_1(\theta_0)]W_{v1}=J(\theta)\theta^2{}_{,\xi}-R^2\cos^2(\psi-\theta)=P \tag{3.3}$$

where P depends on the parameters R, ψ, θ_0 and $k=K_1/K_3$. F is the integral of W_{v1} with respect to z between $z=\pm h$; equivalently,

$$F=[\pi^2 f_1(\theta_0)/4h]\int_{-1}^{+1} P\,d\xi. \tag{3.4}$$

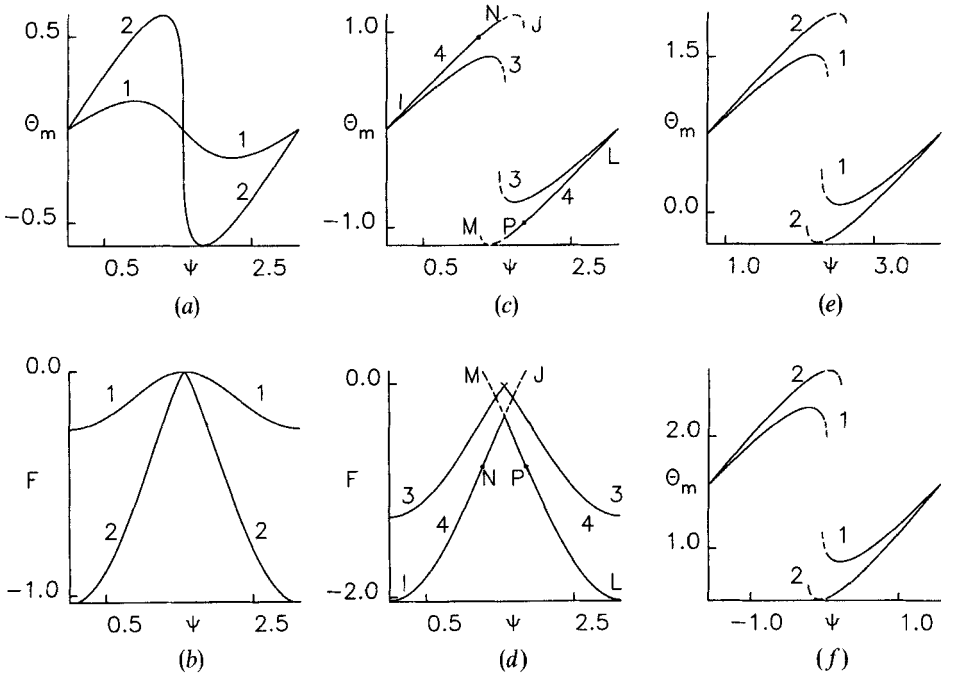

Figure 1. Variation of θ_m and F with ψ for different θ_0 and R. F is the total free energy of the sample (measured in units of 10^{-11} J). The initial uniform orientation $\mathbf{n}_0=(\sin\theta_0, 0, \cos\theta_0)$ in the xz plane is deformed into a symmetric homogeneous distortion $\mathbf{n}=(S_\theta, 0, C_\theta)$, $\theta=\theta(z)$ by the magnetic field $\mathbf{H}=(HS_\psi, 0, HC_\psi)$. $\theta_m=\theta(z=0)$ is the extremum deformation angle at the centre of the sample whose boundaries are at $z=\pm h$ ($=100\ \mu$m). The director is rigidly anchored at the boundaries. $R=H/H_F(\theta_0)$ where $H_F(\theta_0)$ (see equation 3.1) is the Freedericksz threshold for the given configuration. $\mathbf{H}$ is tilted away from $\mathbf{n}_0$ and from $-\mathbf{n}_0$ to get the two different parts of the curves; equivalently, ψ is varied from θ_0 and from $\theta_0\pm\pi$. All angles are measured in radians. Material parameters are given in equations (2.22). $\theta_0=0$. Homeotropic anchoring. ((*a*)–(*d*)) $R=$(1) 0·5, (2) 1·0, (3) 1·1, (4) 1·4. $\theta_0=0{\cdot}75$. (*e*) $R=$(1) 1·1, (2) 1·4. $\theta_0=(\pi/2)$. Homogeneous anchoring. (*f*) $R=$(1) 1·1, (2) 1·4. The F curves have not been shown for (*e*) and (*f*). For $R>1$, there exist two distinct branches of the θ_m and F curves due to bistability. The width of bistability, w_b, increases with R for a given θ_0. For a given R, w_b diminishes when θ_0 is increased from 0 (homeotropic anchoring) to $(\pi/2)$ (homogeneous anchoring). Dashed parts of a curve in the bistable region correspond to distortion states which are more energetic than the corresponding states on the other branch (see § 3.1).

For given k, θ_0 and R the solution from equation (3.2) is independent of h but depends only on ψ. If $h\to h\mu$, the θ_m versus ψ curve will not change if R is held fixed. Due to the property of P from equation (3.3), when $h\to h\mu$, $F\to F/\mu$; thus, the shape of the F versus ψ curve will also not change.

Calculations show that w_b depends strongly on the relative magnitudes of K_1 and K_3 as well as on the particular geometry (i.e. θ_0). In bend geometry ($\theta_0=0$), at fixed R, w_b increases (or decreases) when K_1 is diminished (or enhanced) with respect to K_3. In splay geometry ($\theta_0=\pi/2$), at fixed R, w_b increases (or diminishes) when K_1 is enhanced (or decreased) with respect to K_3. The scaling aspect becomes apparent by noting that $J(\theta)$ is essentially dependent on k as a parameter. Hence, at given R, k and θ_0, the solution from equation (3.2) (and, hence, the θ_m versus ψ curves as well as w_b) will not

depend on the individual values of K_1 and K_3. However, at given R, k, ψ and θ_0, if $(K_1, K_3) \rightarrow \mu''$ (K_1, K_3), then $F \rightarrow \mu''$ F as for equation (3.4).

When $R > 1$, for all practical purposes, the two branches of the theoretical curve represent two distinct sequences of stable distortion states. The limit ψ_c is defined as that limiting value of ψ such that when ψ is increased beyond the limit by a small amount ($\sim 0{\cdot}01$ radian) no further solutions can be found for that branch. In a numerical calculation this can be qualified further. Suppose we change ψ form θ_0 towards $\theta_0 + \pi$. When ψ crosses ψ_c by a small amount the algorithm will either diverge or converge to a deformation state on the other branch.

Experimentally too [13], for $R > 1$, all states on either branch have been recognized to be states of stable deformation as the investigators have allowed sufficient time to elapse after each increment of ψ. Excellent theoretical fits have been obtained for both branches of each curve for $R > 1$. They have also demonstrated that when ψ is changed beyond ψ_c by a small amount ($\Delta\psi$), the distortion on one branch becomes unstable and goes over to the corresponding deformation state on the other branch for fixed R. Typically, for $2h = 370\,\mu$m, $R = 1{\cdot}2$, $\psi_c = 100°$, $\Delta\psi = 5°$ and the time of transition (τ) is ≈ 30 min. A solution of the dynamical equation (2.7), neglecting the coupling between flow and orientation, has led to a description of the rate of change of distortion in good agreement with experiment [13]. A question does arise, however, whether the time of transition can be shortened.

To a certain extent a rigorous solution of the dynamical equations (2.7)–(2.8) should be able to answer the above question; this is not attempted here as it falls outside the scope of the present work. It is, however, possible to utilize physical arguments to derive orders of magnitude for τ, the characteristic time that may be involved in the process. To find out what form τ should have, it is sufficient to note that equations (2.7) and (2.8) can be written in dimensionless form (neglecting inertial terms) as

$$\left.\begin{aligned} &J(\theta)\theta_{,\xi\xi} + \tfrac{1}{2}(dJ/d\theta)\theta^2{}_{,\xi} + \tfrac{1}{2}R^2 \sin(2\psi - 2\theta) - \theta_{,u} - G_2(\theta)V_{x,\xi} = 0; \\ &[G_1(\theta)V_{x,\xi} + G_2(\theta)\theta_{,u}]_{,\xi} = 0; \quad u = t/\tau; \quad \tau = 4h^2\gamma_1/\pi^2 f_1(\theta_0); \\ &V_x = v_x\tau/h; \quad G_1(\theta) = g_1(\theta)/\gamma_1; \quad G_2(\theta) = g_2(\theta)/\gamma_1. \end{aligned}\right\} \tag{3.5}$$

It is seen that the characteristic time τ scales as h^2. It has already been noted that w_b depends only on R regardless of the sample thickness. It may now be stated tentatively that for a given R, the transition time (for instance from J to P or from M to N; see figures 1 (*c*) and (*d*)) may be shortened if one uses a thinner sample; this fact is also capable of experimental verification.

It appears at this stage that a linear stability analysis would be a convenient way to investigate the dynamics that might occur near the edges of the bistable region. Such an exercise is slightly complicated in the splay/bend geometry due to the unavoidable coupling between the director and velocity perturbations. It shall be seen later (see section 5.2) that perturbation analysis can be achieved more conveniently in another situation.

3.2. *Non-symmetric director tilt at the sample planes; rigid anchoring*

The initial director field from equation (2.3) is now a function of z as $\theta_\pm$ are not equal as from equations (2.1) and (2.11). On such a configuration, **H** is imposed at same angle ψ with respect to z in the xz plane and ψ is slowly varied. There is no threshold in this geometry as **H**, applied at any ψ, will only change the existing distortion. As θ is an asymmetric function of z, the angle at the sample centre $\theta_c = \theta(z = 0)$ is not an extremum.

It is found that two kinds of deformation are possible depending upon the values of R, ψ and $\theta_{\pm}$.

(i) In the first, which we shall call $\mathscr{D}_1$, θ varies monotonically from θ_- at $z=-h$ to θ_+ at $z=+h$.

(ii) In the second, denoted by $\mathscr{D}_2$, θ shows an extremum θ_m at some $z=z_m$, $-h<z_m<h$. In principle θ_m can be used for representing the extent of deformation. But the solution $\mathscr{D}_2$ occurs only over limited ranges of ψ for given R and $\theta_{\pm}$. Hence, it is convenient to use θ_c to represent the amount of distortion.

A variety of combinations of $\theta_{\pm}$ can be chosen to yield a non-symmetrically distorted ground state. To simplify matters, θ_- is taken to be $(\pi/2)$ (homogeneous anchoring at $z=-h$) and different values are chosen for θ_+ in the range $0<\theta_+<(\pi/2)$. As θ_- is fixed, the splay threshold $H_F(\pi/2)$ can be employed to provide a measure of H.

For the uniformly tilted case (see figure 1) it was sufficient to start with **H** along $\mathbf{n}_0$ (or along $-\mathbf{n}_0$) and change ψ over π radian. Because $\theta_- \neq \theta_+$ in the present case, there does arise some ambiguity about the range over which ψ should be varied and also about the initial and final values of ψ. To settle this, first the θ_c versus ψ plots are shown in figures 2 (*a*)–(*d*) for different $R=H/H_F(\pi/2)$ and $\theta_+=0{\cdot}8$; ψ is varied over a range of

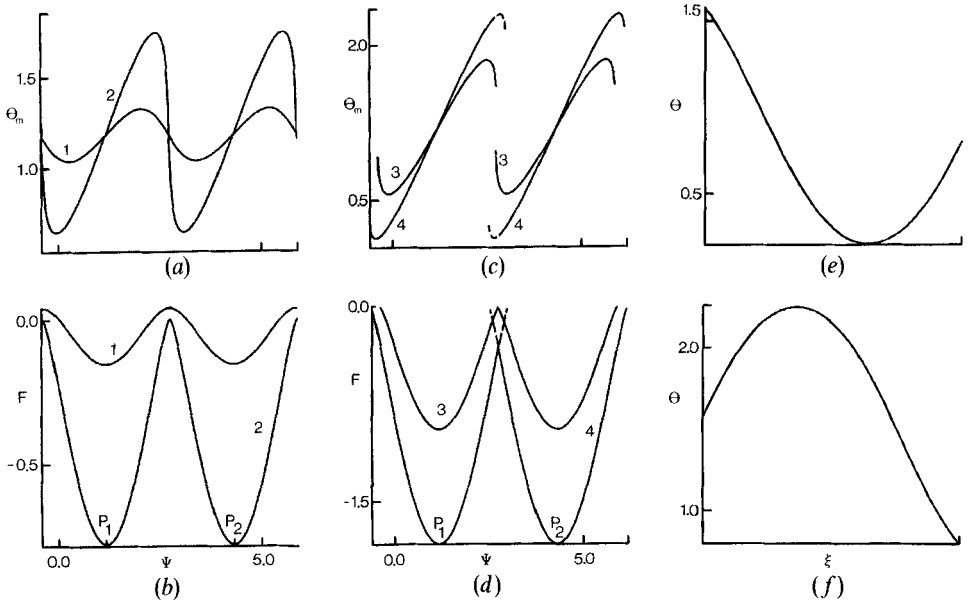

Figure 2. Plots of θ_c and F versus ψ for different R and examples of the asymmetric $\mathscr{D}_2$ profiles. Rigid anchoring $\theta=\theta_{\pm}$ at $z=\pm h$(or $\xi=\pm 1$) so that the ground state from equation (2.3) is asymmetric even in the absence of **H**. $\theta_-=(\pi/2)$, $\theta_+=0{\cdot}8$ radian in all cases. $R=H/H_F(\pi/2)$ where $H_F(\pi/2)$ is the splay Freedericksz threshold from equation (3.1). $\theta_c=\theta(z=0)$ is not the extremum of $\theta(z)$. (*a*)–(*d*) $R=(1)\,0{\cdot}5\,(2)\,1{\cdot}0,(3)\,1{\cdot}1,(4)\,1{\cdot}5$. The ψ range P_1P_2 ($=\pi$ radian) is sufficient to give a proper representation of bistability. The actual position of P_1 (and, hence, P_2) is a function of R, $\theta_{\pm}$. (*e*) and (*f*) The asymmetric θ profile exhibits an extremum ($\mathscr{D}_2$ profile) over limited ranges of ψ for given R and $\theta_{\pm}$. Two examples are given. $R=1{\cdot}5$, $\psi=$(*e*) $-0{\cdot}6$, (*f*) 3·01 radian. Bistability should be observable even in cases where a Freedericksz threshold cannot be defined (see § 3.2).

about 2π. It is immediately apparent that the results are amply represented by varying ψ between the minima of F (P_1 to P_2). The parts of curves outside this range can be generated by reflection of each part of the curve (in the P_1P_2 region) in suitable mirror planes. Further, the gap P_1P_2 is found to be π radian (perhaps due to non-polarity). The positions of P_1 and P_2 on the ψ axis depend on R and on θ_+, for a given θ_-. Figures 2 (*e*) and (*f*) also give the representative $\mathscr{D}_2$ profiles in two situations where θ exhibits extrema. It is thus clear that bistability and discontinuous orientational changes are possible even in a situation where no threshold can be defined.

Figures 3 (*a*)–(*c*) contain plots of θ_c against ψ for $\theta_- = (\pi/2)$ and three different θ_+. As there is no bistability for $R \leqq 1$, only two values of $R > 1$ have been chosen. The F plots have not been included as their shape is similar to the F plots shown in figures 1 and 2. It is seen that as θ_+ diminishes (i.e. as the amount of initial deformation in the sample increases) w_b decreases. When R is sufficiently small bistability may even be suppressed altogether by sufficiently enhancing the asymmetry between the director tilts at the sample planes.

Another non-symmetric configuration that comes to mind is the reversely pretilted orientation at the sample planes. Though a number of different tilts are possible in this case, we shall confine our attention to the case $\theta_\pm = \pm\theta_0 + (\pi/2)$, where θ_0 is an acute angle. The starting configuration (from equation (2.3)) is again a function of z but now

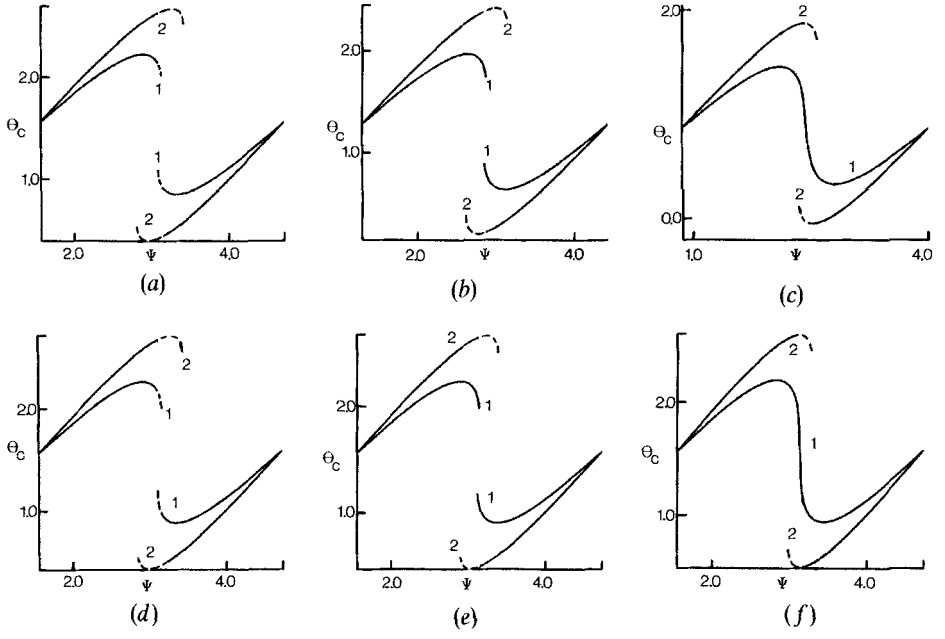

Figure 3. Variation of θ_c as a function of ψ for non-symmetric director tilt at the boundaries. Rigid anchoring. Plots of F have not been included but the more energetic states have been shown by dashed lines in the bistable region. (*a*)–(*c*) $\theta_- = (\pi/2)$ (homogeneous alignment at $z = -h$). $\theta_+ =$ (*a*) 1·5 (*b*) 1·0 (*c*) 0·2 radian. $R = H/H_F(\pi/2)$. Curves have been drawn for $R =$ (1) 1·1, (2) 1·5. Bistability is found not to occur for $R \leqq 1$, hence these results have not been included. Enhancement of the ground state distortion is detrimental to the occurrence of bistability. (*d*)–(*f*)) $\theta_\pm = \pm\theta_0 + (\pi/2)$; reversely pretilted ground state. $R = H/H_F(\theta_0)$ (see equation (3.1)). Curves have been drawn for $R =$ (1) 1·1, (2) 1·5. $\theta_0 =$ (*d*) 0·1, (*e*) 0·4, (*f*) 0·7 radian. The conclusions are similar to those of (*a*)–(*c*) (see § 3.2).

$\theta-(\pi/2)$ and, therefore, n_x are antisymmetric with respect to $z=0$. **H** is impressed on such a configuration in the xz plane and ψ is varied. Results are presented for this case in figures 3(*d*)–(*f*) without going into the details of the stability of the initial configuration.

As $\theta_\pm = \pm\theta_0+(\pi/2)$ are equally spaced with respect to $(\pi/2)$ and also because **n** at the sample centre is initially along x, it is obvious that $(\pi/2)\leqq\psi\leqq(3\pi/2)$ should serve as an adequate ψ range for describing the variation of deformation; this point has been checked numerically. In this case, again, there is no threshold for any ψ. To provide a measure for H, the value $H_F(\theta_0+\pi/2)=H_F(-\theta_0+\pi/2)$ from equation (3.1) can be chosen.

In the absence of **H**, $n_x(z)$ is antisymmetric; once **H** is impressed on the sample, the director profile becomes asymmetric. As in the previous case, only over certain ψ ranges, the distortion exhibits the $\mathscr{D}_2$ type of profile. Again, therefore, $\theta_c=\theta(z=0)$ is used for describing the extent of distortion in the sample. As bistability is not discernible for $R\leqq 1$, only values of $R>1$ have been used. The conclusion of figures 3(*d*)–(*f*) are similar to those of figures 3(*a*)–(*c*); enhancement of the distortion in the initial configuration is deleterious to the occurrence of bistability.

3.3. *Uniform tilted orientation at the sample planes; weak anchoring*

The easy axes at the sample planes as well as the initial orientation are given by equation (2.1) with $\theta_\pm=\theta_0$. Under the action of **H** from equation (2.2), the deformation from equation (2.3) is described by the static part of equation (2.7) subject to the boundary conditions from equation (2.10). The initial task is to estimate the threshold for this case. This is conveniently achieved by linearizing equations (2.7) and (2.10) with respect to the perturbation $\theta''=\theta(z)-\theta_0$ for $\psi=\theta_0+(\pi/2)$ from equation (2.2)

$$\left.\begin{aligned}&\theta''_{,\xi\xi}+q^2\theta''=0:\quad[\theta''_{,\xi}\pm\sigma_{\theta\pm}\theta''](\xi=\pm1)=0;\\&\sigma_{\theta\pm}=hB_{\theta\pm}/f_1(\theta_0);\quad q^2=\mu_0\chi_a H^2h^2/f_1(\theta_0).\end{aligned}\right\}\tag{3.6}$$

It must be remembered that for weak anchoring at the boundaries restrictions are placed on the derivative of θ'' and not on θ'' itself. It is convenient to solve initially for the case of equal anchoring strengths at the sample planes.

With $\sigma_{\theta\pm}=\sigma_\theta$, equation (3.6) supports two independent modes: Mode H_1 (or Mode H_2) with θ'' even (or odd) with respect to the sample centre. Taking $\theta''\approx\cos q\xi$, equation (3.6) reduces to the compatibility condition for Mode H_1

$$C_1=\sigma_\theta\cos q-q\sin q=0\tag{3.7}$$

from which $q_c(0<q_c<\pi/2)$ and hence the threshold

$$H_F\equiv H_F(\theta_0,B_\theta)=(q_c/h)[f_1(\theta_0)/\mu_0\chi_a]^{1/2}\tag{3.8}$$

can be determined. For rigid anchoring, $\sigma_\theta\gg1$ and $q_c\approx(\pi/2)$ as it should. When B_θ is diminished (when the anchoring is weakened) q_c and, therefore, H_F decrease for a given material and sample thickness.

For Mode H_2, with $\theta''\approx\sin q\xi$, the compatibility condition of equation (3.6) reduces to

$$C_2\equiv\sigma_\theta\sin q+q\cos q=0\tag{3.9}$$

which, of course, yields a higher $q_c(\pi/2<q_c<\pi)$ and, therefore, a higher threshold (which is only of academic interest).

For asymmetric anchoring at the sample planes ($\sigma_{\theta+} \neq \sigma_{\theta-}$),

$$\theta'' \approx \theta''_S \sin q\xi + \theta''_c \cos q\xi$$

is asymmetric with respect to $z=0$; θ_S, θ''_c are indeterminate, infinitesimal amplitudes. The compatibility condition for equation (3.6) becomes

$$C_{12} = (\sin 2q)(q^2 - \sigma_{\theta+}\sigma_{\theta-}) - q(\cos 2q)(\sigma_{\theta+} + \sigma_{\theta-}) = 0 \tag{3.10}$$

from which q_c can be found; substitution in the right hand side of equation (3.8) leads to H_F for the asymmetric case, with H_F depending on both anchoring strengths. It may be checked that putting $\sigma_{\theta+} = \sigma_{\theta-} = \sigma_\theta$ in equation (3.10) and factorizing leads to

$$C_{12} = C_1 C_2 = 0. \tag{3.11}$$

As the zero of C_1 corresponds to the lower q_c of equation (3.7), equation (3.11) will again lead to the Mode H_1 threshold from equation (3.8).

For the sake of simplicity, anchoring strengths of the two boundaries are assumed to be equal. For given B_θ and other parameters, H_F is calculated from equations (3.7) and (3.8). It is possible to consider different initial pretilt angles, θ_0, as shown in figure 1. However, only the homeotropic pretilt is studied; $\theta_0 = 0$. As the distortion for any value of H and ψ is symmetric, $\theta_m = \theta(z=0)$ is an extremum and serves to measure the amount of deformation. Once distortion occurs in the sample, the elastic torques acting at the surface produce a change in the tilt of $\mathbf{n}$ at the surfaces away from the free axes. As the deformation is symmetric, θ at either boundary will be equal; $\theta(z = \pm h) = \theta_S$. Figures 4 (*a*)–(*d*) show the variation of θ_m with ψ for different anchoring strengths B_θ. The starting value of ψ is 0 or π. Bistability does not appear for $R \leqq 1$. F is calculated (see § 2.3) by adding the surface and volume contributions. The shape of the F versus ψ curves is found to be similar to that of the curves shown previously.

At small R (e.g. $R = 1{\cdot}1$), w_b is hardly affected by a change in B_θ; for $R = 1{\cdot}5$, however, the change is more pronounced quantitively as well as qualitatively. When B_θ is decreased from 10^{-5} to 3×10^{-7} N m^{-1}, w_b hardly changes (these results have not been displayed). In this range of B_θ, q_c from equation (3.7) does not change appreciably from $(\pi/2)$. When B_θ is diminished further, w_b increases (see figures 4 (*a*) and (*b*)); this is also accompanied by a corresponding increase in $|\theta_m|$. When B_θ is decreased further to 10^{-7} N m^{-1}, this trend is reversed and w_b starts to diminish (see figure 4 (*c*)). When B_θ is decreased still further (to $0{\cdot}5 \times 10^{-7}$ N m^{-1}), $w_b \to 0$ and a new behaviour is evident; θ_m changes sign discontinuously as ψ crosses $(\pi/2)$ (see figure 4 (*d*)).

To understand this more completely, θ_m and θ_S have been plotted as functions of ψ for $R = 1{\cdot}5$ and two values of B_θ. When $B_\theta = 2 \times 10^{-7}$ N m^{-1} (see figure 4 (*f*)) there exists considerable difference between θ_m and θ_S in the region of bistability showing that the surface continues to control the deformation. At $B_\theta = 10^{-7}$ N m^{-1} (see figure 4 (*e*)) θ_S tends to approach θ_m in the region of bistability; it is clear that the surface has started to yield to the dictates of the distortion in the bulk.

It is necessary, therefore, to appreciate the two different ways in which anchoring strength can affect bistability. When B_θ is initially decreased from the rigid anchoring limit, the tilt at the surface can change sufficiently away from the easy axis as $\mathbf{H}$ is rotated away from $\mathbf{n}_0$ so that the total amount of distortion is reduced; this partial yielding at the surface can actually enhance the width of bistability. When B_θ is reduced considerably we reach the other limit. If R is high enough there may occur a tendency for $\mathbf{n}$ in a large portion of the sample to turn towards $\mathbf{H}$ as the tilt of $\mathbf{H}$ with respect to the easy axes of the plates exceeds a critical value; this may actually deter bistability.

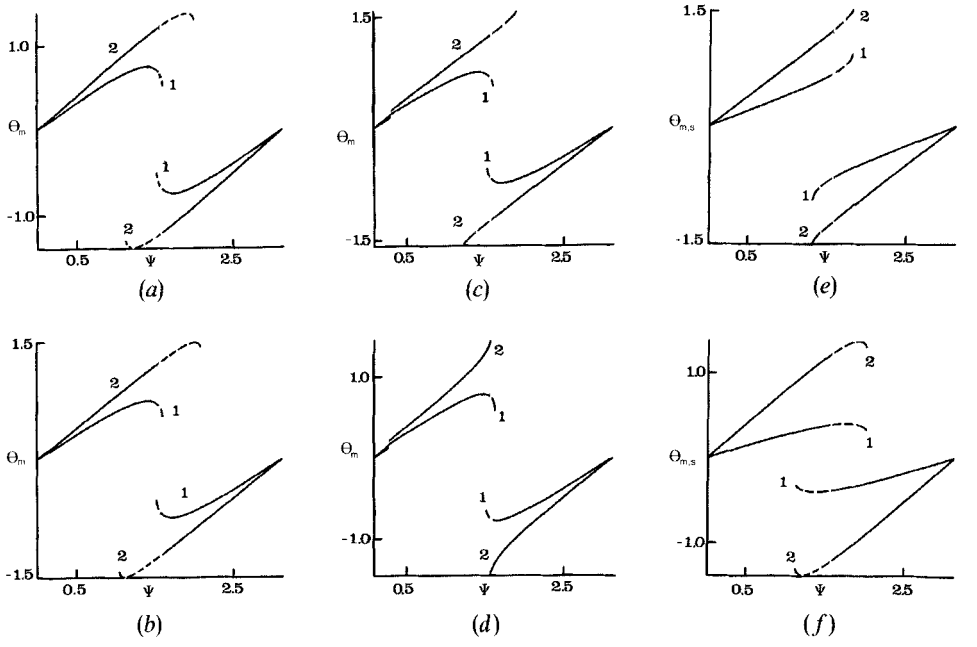

Figure 4. Plots of θ_m and θ_S versus ψ for different R and B_θ. Weak anchoring at the sample planes. Easy axes at the sample planes and initial uniform alignment are homeotropic ($\theta = 0$). B_θ is the anchoring strength at either boundary. $R = H/H_F(B_\theta)$ where $H_F(B_\theta)$ is the Freedericksz threshold calculated, for a given B_θ, from equations (3.7) and (3.8). θ_m is the extremum distortion angle at the sample centre. Dashed lines in the bistable region indicate states of higher total free energy F which is now calculated as the sum of volume and surface contributions. The variation of F has not been shown. Again, bistability is found not to set in for $R \leqq 1$. (*a*)–(*d*) θ_m versus ψ. $R = (1)$ 1·1, (2) 1·5. $B_\theta = (a)$ 2·0, (*b*) 1·3, (*c*) 1·1, (*d*) 0·5 (in units of 10^{-7} N m^{-1}). The bistable behaviour for $R = 1{\cdot}1$ is hardly affected but that for $R = 1{\cdot}5$ exhibits some variation. w_b may increase or decrease with respect to the rigid anchoring value depending upon the magnitude of B_θ. (*e*) and (*f*) θ_m (see curves 2) and θ_s (see curves 1) versus ψ for $R = 1{\cdot}5$. θ_s is the director tilt angle with respect to the easy axis at the sample planes (as the anchoring is weak, θ_s does not remain fixed at $\theta_0 = 0$ but varies, depending upon the extent of distortion in the bulk). The indications are clear that if B_θ is small enough and R sufficiently high, a discontinuous transition may occur from a deformed state of orientation to an aligned state (with the director everywhere parallel to **H**) when ψ exceeds some limit (see § 3.3).

Calculations have shown that when B_θ is very small ($\sim 10^{-8}$ Nm^{-1}), θ_m and θ_S may jump discontinuously to ψ as ψ is changed beyond a certain limit. Outside this limit, deformation disappers with θ becoming equal to ψ in the entire sample. This actually indicates the possibility of the occurrence of a discontinuous transition from a deformed state to a state of uniform alignment (in the entire sample) which follows. **H**. The possibility cannot be ruled out that this transition may even be realizable at higher B_θ when R is sufficiently large. Detailed calculations of this case will be presented separately.

3.4. *Twist geometry; rigid anchoring*

It is proposed to study the solutions of the static part of equation (2.19) with the boundary conditions from equation (2.21). As the ground state is uniformly twisted, we can set $\phi_\pm = \pm\phi_0$ without loss of generality. Then in the field free limit, **n** at the sample

centre is oriented along the y axis. Because of the (anti-) symmetry of the ground state, the relevant range for field tilt is $0 \leqq \psi \leqq \pi$ (i.e. **H** is rotated away from $+y$ or $-y$ in the xy plane). The untwisted ground state ($\phi_0 = 0$) is a special case. The cases of a twisted nematic and a chiral nematic are illustrated separately.

When $\phi_0 = 0$, the ϕ profile is symmetric with respect to $z = 0$ at any H and ψ; hence, $\phi_m = \phi(z=0)$ can be employed as a distortion measure. In all other cases the deformation is asymmetric (as in § 3.2 we again encounter the $\mathscr{D}_2$ type ϕ profiles over limited ranges of ψ) so that one studies $\phi_c = \phi(z=0)$. H is conveniently measured in terms of the twist threshold $H_T = (\pi/2h)(K_2/\mu_0\chi_a)^{1/2}$. While calculating F, k_2 is assumed to be zero. Bistability is found not to occur for $R \leqq 1$, hence only $R > 1$ is chosen. The results of figure 5 (*a*) are similar to those of figure 1. Figures 5 (*b*) and (*c*) indicate that an

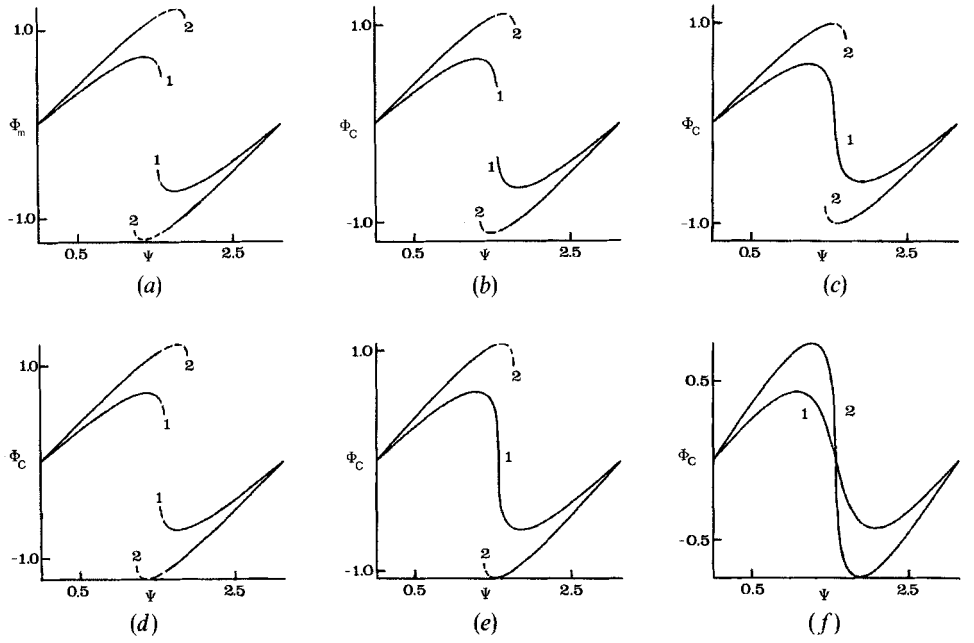

Figure 5. Twist deformations. Variation of ϕ_m, ϕ_c as functions of ψ for different R and ϕ_0. The ground state is uniformly twisted with the helical axis along z such that $\mathbf{n}_0 = (S_\phi, C_\phi, 0)$ where $\phi = \phi(z)$. At the boundaries $z = \pm h$, **n** is rigidly anchored along $(\pm \sin\phi_0, \cos\phi_0, 0)$ so that $2\phi_0$ is the total twist angle of the ground state and **n** at the sample centre is along y. $\mathbf{H} = (HS_\psi, HC_\psi, 0)$ is applied in the xy plane and ψ is varied between 0 and π. $R = H/H_T$ where H_T is the twist Freedericksz threshold. $R \leqq 1$ is of no interest from the viewpoint of bistability. Curves are drawn for $R = (1)$ 1·1. (2) 1·5, in all diagrams. $\phi_0 = (a)$ 0·0 (untwisted homogeneously aligned ground state), (*b*) 0·5, (*c*) 0·75 radian. (*a*) ϕ_m versus ψ. $\phi_m = \phi(z=0)$ is the maximum distortion angle of the symmetric director profile. (*b*) and (*c*) ϕ_c versus ψ. $\phi_c = \phi(z=0)$. The ϕ profiles are asymmetric with respect to the sample centre. (*d*)–(*f*) ϕ_c versus ψ for a cholesteric of equilibrium pitch $2\pi h/\phi_0$. The initial configuration is the same as that for (*a*)–(*c*). While calculating F for this case it is necessary to add the term proportional to $k_2 = (K_2\phi_0/h)$ to the free energy density. $\phi_0 = (d)$ 0·1, (*e*) 0·6, (*f*) 1·2 radian. An increase in the ground state twist deters the occurrence of bistability. By suitably changing the markings on the ψ axis, the above results can be taken over to the case of a $\chi_a < 0$ nematic. As in figures 2 and 3, it must be remembered that a Freedericksz field cannot be defined for a rigidly anchored chiral nematic with **H** acting normal to the helical axis. The results of figure 5 are valid for any material and depend only on R, h and the boundary values (see § 3.4).

increase in the ground state deformation can even suppress bistability when R is not large.

The twisted nematic has the inherent limitation that the total twist of the ground state cannot exceed $(\pi/2)$. This limitation can be overcome by using either a cholesteric or a chiral nematic. For the sake of simplicity the same assumption is carried over here for the ground state; we effectively assume that the ground state is a cholesteric which retains its equilibrium pitch $= 2\pi h/\phi_0$ while being rigidly anchored at the sample planes [29]. The k_2 term ($k_2 = K_2\phi_0/h$) is included while calculating F. Figures 5(*d*)–(*f*) reaffirm the conclusions of figures 5(*a*)–(*c*). Interestingly, bistability may be removed even at $R = 1{\cdot}5$ by employing a sufficiently high initial twist unattainable in a twisted nematic. It should be remembered that when **H** is applied normal to the helical axis of a chiral nematic there is no deformation threshold. This is again a demonstration that bistability can occur even in the absence of a symmetry breaking Freedericksz transition.

It is worth noting that the static part of equation (2.19) along with equation (2.21) can be recast into the form

$$\phi_{,\xi\xi} + (\pi^2 R^2/4)\sin(\psi - \phi)\cos(\psi - \phi) = 0; \quad \phi(\xi = \pm 1) = \phi_{\pm}. \tag{3.12}$$

This only means that the solution $\phi(\xi)$ depends on ψ, R and on the boundary values for any material provided that anchoring is rigid. The results of figure 5 should be interpreted in this light.

The twisted ground state is a generalization of the untwisted (homogeneously aligned) state in the twist case just as the non-symmetric ground state is a generalization of the uniformly tilted (homogeneous or homeotropic) ground state in the splay/bend geometry. Still, one difference remains. In the splay/bend case the antisymmetrically distorted ground state can be distinguished from the asymmetrically defomed one depending upon the $\theta_{\pm}$ values at the boundaries. In the twist case $\phi(z)$ of the ground state varies linearly with z whatever the value of $\phi_{\pm}$; hence, the coordinate system can always be rotated about the z axis by a suitable angle to bring the y axis parallel to **n** at the sample centre. Thus the most general ground state in the twist case is antisymmetric. Obviously the effects of weak anchoring on bistability can be expected to be similar to those in the splay/bend case.

4. Effect of an additional electric field E

So far only the effect of **H** on the orientation has been studied. In this section the action of an additional static **E** will be included to find out how **H** induced bistability is influenced. Two convenient ways of impressing **E** on a sample present themselves. In the first, a voltage V is applied between plates $z = \pm h$ whose inside surfaces, coated with conducting layers, act as electrodes. In this case **E**, having the constant value $V/2h$, will act normal to the plates in the absence of deformation. This geometry can be conveniently studied by a slight generalization of the picture developed in [15] to include magnetic terms; these results will be presented separately.

In the second case the voltage V is impressed between electrodes $x = \pm g$ which sandwich the nematic cell. In the absence of distortion **E**, having the constant value $V/2g$, acts along the x axis. In this section some results are presented for this case. A brief description of the derivation of the governing equations is given on the basis of previous work [16–18].

4.1. *Governing equations for* **E** *applied parallel to the plates*

The interelectrode gap ($2g$) is assumed to be large compared to the sample thickness ($2h$). Then by considering regions of the sample far away from the electrodes the distortion can be assumed to be homogeneous. The director field is defined by equations (2.1) and (2.3). Together with Maxwell's curl equation the boundary conditions on **E** imply that

$$\mathbf{E}=[E_x, 0, E_z(z)]; \quad E_x=\text{constant}. \tag{4.1}$$

The boundary condition on the electric induction **D**, along with Maxwell's divergence equation, implies that $D_z=0$ in the sample; this leads to an expression for E_z

$$E_z=S_\theta C_\theta[\{(e_1+e_3)\varepsilon_0\}\theta_{,z}-\varepsilon_a E_x]/f_2(\theta); \quad f_2(\theta)=\varepsilon_\perp+\varepsilon_a C_\theta^2, \tag{4.2}$$

where e_1 and e_3 are flexoelectric coefficients; $\varepsilon_\parallel$ and $\varepsilon_\perp$ the dielectric constants along and normal to **n**, respectively; $\varepsilon_a=\varepsilon_\parallel-\varepsilon_\perp$. As V, the potential difference, is held constant the term W'' [3, 15]

$$\left.\begin{aligned} &W''=-P_iE_i-\varepsilon_0\varepsilon_{ij}E_iE_j/2;\\ &\varepsilon_{ij}=\varepsilon_\perp\delta_{ij}+\varepsilon_a n_i n_j; \quad P_i=e_1 n_i n_{k,k}+e_3 n_k n_{i,k} \end{aligned}\right\} \tag{4.3}$$

is added to the right-hand side of W_{v1} in equation (2.5); ε_{ij} is the dielectric tensor and P_i the flexoelectric polarization. The equations of equilibrium result from a minimization of W_{v1}

$$\left.\begin{aligned} &f_3(\theta)\theta_{,zz}+\tfrac{1}{2}(df_3/d\theta)\theta^2_{,z}+\tfrac{1}{2}\mu_0\chi_a H^2\sin(2\psi-2\theta)\\ &\qquad+E_x^2 S_\theta C_\theta\varepsilon_a\varepsilon_\perp\varepsilon_\parallel\varepsilon_0/f_2^2(\theta)=0;\\ &f_3(\theta)=f_1(\theta)+(e_1+e_3)^2 S_\theta^2 C_\theta^2/\varepsilon_0 f_2(\theta). \end{aligned}\right\} \tag{4.4}$$

Flexoelectricity contributes a volume effect just as it does in the other configuration [15]. In the limit of small distortions the flexoelectric contribution vanishes from equation (4.4). But when the deformation is large, flexoelectricity can influence the bulk free energy through a normalization of the elastic constants. For weak anchoring the boundary conditions are as from equation (2.10) except that

$$\partial W_{v1}/\partial\theta_{,z}=f_3(\theta)\theta_{,z}+f_4(\theta)E_x; \quad f_4(\theta)=(e_1\varepsilon_\perp S_\theta^2-e_3\varepsilon_\parallel C_\theta^2)/f_2(\theta). \tag{4.5}$$

For the sake of simplicity flexoelectricity is assumed to be absent ($e_1=e_3=0$). The anchoring is also taken to be rigid from equation (2.11) [35]. In principle, $\theta_\pm$ can assume any value. For the present we shall confine our attention to two simple cases of initial homeotropic alignment along z ($\theta_\pm=0$) and initial homogeneous tilt along x ($\theta_\pm=\pi/2$). This also ensures that the distortion will be symmetric.

It is straightforward to show that in the bend geometry the second order (electric) threshold is given by [16–18]

$$\left.\begin{aligned} &E_B=(\varepsilon_\parallel K_3\zeta^2/\varepsilon_0\varepsilon_\perp\varepsilon_a h^2)^{1/2}; \quad \zeta^2>0;\\ &\zeta^2=\pi^2/4 \quad \text{if} \quad H=0;\\ &\zeta^2=(\pi^2/4)+(\mu_0\chi_0 h^2H^2/K_3) \quad \text{if} \quad \psi=0;\\ &\zeta^2=(\pi^2/4)-(\mu_0\chi_a h^2H^2/K_3) \quad \text{if} \quad \psi=\pi/2. \end{aligned}\right\} \tag{4.6}$$

It is natural to use $E_B(H=0)$ as a measure of E in the bend geometry.

Similarly in the splay geometry the second order splay (magnetic) threshold is

$$H_S=[\{(\pi^2K_1/4h^2)+(\varepsilon_0\varepsilon_a\varepsilon_{\|}E_x^2/\varepsilon_{\perp})\}/\mu_0\chi_a]^{1/2}. \tag{4.7}$$

The equation for twist distortion takes an especially simple form [18] when $2g \gg 2h$. The boundary conditions on **E** and **D**, along with Maxwell's equations, demand that $E_x=$ constant, $E_y=0$ and $E_z=0$. This amounts to adding $\{-(\varepsilon_{\|}S_\phi^2+\varepsilon_{\perp}C_\phi^2)\varepsilon_0E_x^2/2\}$ to the right-hand side of W_{v2} from equation (2.17) and $(\varepsilon_0\varepsilon_aE_x^2S_\phi C_\phi/2)$ to the left-hand side of (2.19). As it will become clear, some results for this case can be deduced by analogy from those for the splay/bend geometry. Hence, a detailed study of the effects of **E** on bistability of twist distortions will not be presented here.

4.2. *Results for rigid anchoring; splay/bend geometry*

Previous studies have shown [16–18] that the effect of **E** on deformation may depend strongly on the magnitude of ε_a even in the absence of **H**. In the same way, the value of ε_a can be expected to determine the way in which **E** affects **H** induced bistability. The initial task, therefore, is to make a proper choice of $\varepsilon_{\|,\perp}$ before taking up model calculations.

The values [16, 18]

$$\varepsilon_{\|,\perp}=18{\cdot}8,\ 8{\cdot}2 \tag{4.8}$$

are used along with those of the remaining parameters from equation (2.22). In the bend geometry this leads to the familiar discontinuous transition (see curve 1 in figure 6(*a*)) when θ_m is plotted against $r_E=E_x/E_B(H=0)$ from equation (4.6). The dashed curves in the region of bistability indicate states of higher F. When ε_a is diminished (see curves 2 and 3 in figure 6(*a*)) the transition width decreases and finally (see curve 4) the transition becomes continuous [16–18].

The results of figures 6(*b*) and (*c*) are analogous to those of figure 6(*a*). The initial alignment being homogeneous (along x), E_x has a stabilizing influence. With **H** impressed along z, θ_m is plotted as a function of $R=H/H_S$ from equation (4.7). When ε_a is high enough and E_x sufficiently stabilizing, the **H** induced splay transition becomes discontinuous (see figure 6(*b*). At a given stabilizing E_x the transition can be made continuous by decreasing ε_a (see figure 6(*c*)). These results are in agreement with the predictions of [17].

It should be remembered that figures 6(*a*)–(*c*) represent one of the domains of distortion; the deformation in the other domain can be obtained by using the horizontal axis as a mirror plane. The continuity or otherwise of the transition can be controlled if it is possible to vary the value of ε_a. It is known that diminution of ε_a can be achieved, at a given temperature, by using time varying **E** of sufficiently high frequency if the nematic is known to exhibit strong dielectric relaxation. It is also possible to decrease ε_a by heating the nematic towards the isotropic point [36]; in this case if an exact calculation were to be performed, it would be necessary to use the actual values of K_1 and K_3 at different temperatures.

Figures 6(*d*)–(*f*) illustrate the rather obvious effect of a stabilizing E_x on **H** induced bistability in a sample with initial homogeneous alignment along x. The strength of **E** is measured in terms of r_E defined earlier. $R=H/H_F(\pi/2)$, where $H_F(\pi/2)$ is the splay threshold. An increase in r_E diminishes w_b. For equation (4.8) bistability disappears at $R=1{\cdot}5$ when $r_E=0{\cdot}5$ (see figure 6(*d*)). When ε_a is lower (see figures 6(*e*) and (*f*) bistability is removed by choosing a higher r_E. The action of the stabilizing E_x is to enhance the effective threshold H_S from equation (4.7) in the splay geometry. Hence, if

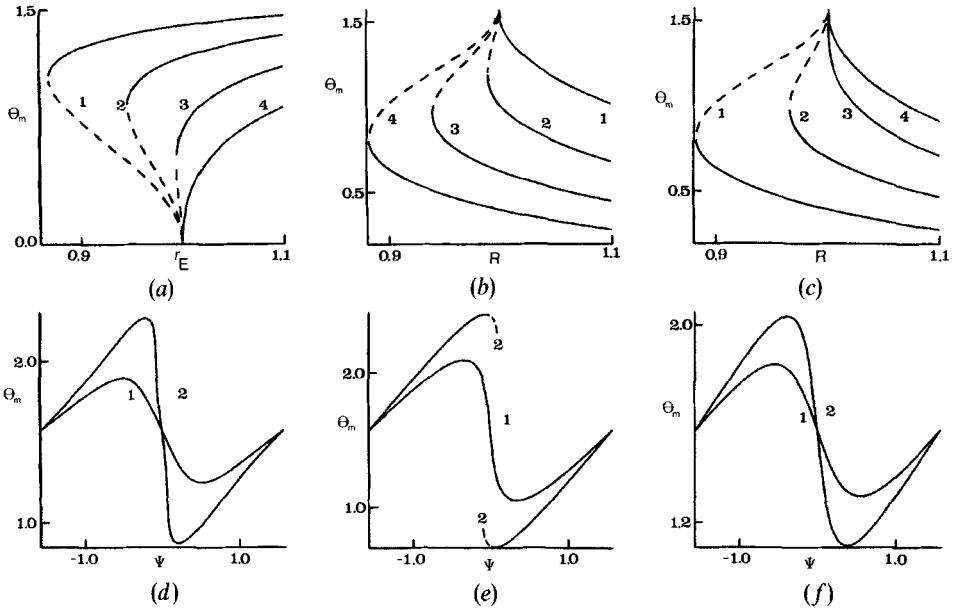

Figure 6. (*a*)–(*c*) Electric field induced bend transition; effect of **E** on the **H** induced splay transition. Rigid anchoring. Only one of the possible two domains is represented in each diagram. **E** is impressed along x parallel to the plates $z = \pm h$. The results are in agreement with those of [16–18]. (*a*) θ_m versus r_E in the bend geometry; $H = 0$. Initial orientation is homeotropic, along z. $r_E = E_x/E_B(H=0)$ where the denominator is the second order bend threshold from equation (4.6). Curves are drawn for $\varepsilon_{\|}, \varepsilon_{\perp} =$ (1) 18·8, 8·2, (2) 17·48, 9·53, (3) 16·15, 10·85, (4) 14·83, 12·18 [37]. As ε_a is diminished, the transition turns continuous. (*b*) and (*c*) Homogeneous initial alignment along x. E_x has a stabilizing influence. For **H** acting along z there exists a second order Freedericksz threshold H_S from equation (4.7). $R = H/H_S$. (*b*) θ_m versus R for $\varepsilon_{\|}, \varepsilon_{\perp} = 18{\cdot}8, 8{\cdot}2$. $E_x =$ (1) 0·0, (2) 0·15, (3) 0·225, (4) 0·3 (in units $10^4\ \mathrm{V\,m^{-1}}$). When the stabilizing **E** is strong enough, the **H** induced splay threshold becomes discontinuous. (*c*) θ_m versus R for $E_x = 0{\cdot}3 \times 10^4\ \mathrm{V\,m^{-1}}$. The values of $\varepsilon_{\|}$ and $\varepsilon_{\perp}$ are as in figure (*a*). Diminution of ε_a, at a given stabilizing E_x, causes the **H** induced splay transition to turn continuous. (*d*)–(*f*) Homogeneous initial alignment along x. **E** is impressed along x. $R = H/H_F(\pi/2)$ where $H_F(\pi/2)$ is the splay Freedericksz threshold. From equation (3.1) r_E is defined as in figure (*a*). Curves are drawn for $R =$ (1) 1·1, (2) 1·4. $\varepsilon_{\|}, \varepsilon_{\perp} =$ (*d*) 18·8, 8·2, (*e*) and (*f*) 14·83, 12·18. $r_E =$ (*d*) 0·5 (*e*) 0·5 (*f*) 1·0. A stabilizing **E** enhances the effective splay Freedericksz threshold H_S from equation (4.7). Hence at a given H, bistability can be removed by using a sufficiently high E (see § 4.2).

H is kept constant and E_x sufficiently increased so that $H < H_S$, bistability will disappear. It is quite possible that a stabilizing **E**, applied to normal to the plates, may have a similar influence on **H** induced bistability for initial homeotropic alignment.

In contrast, **E** has a destabilizing influence in the bend geometry so that the effective bend magnetic threshold

$$H_B = [\{(K_3\pi^2/4h^2) - (\varepsilon_0\varepsilon_a\varepsilon_\perp E_x^2/\varepsilon_{\|})\}]/\mu_0\chi_a]^{1/2} \tag{4.9}$$

decreases from $H_F(0)$ from equation (3.1). Hence, w_b can be expected to increase when r_E is enhanced. In particular, if $R = H/H_F(0)$ then bistability should set in even for $R \leqq 1$.

Figures 7 (*a*)–(*f*) illustrate these effects for two different values of ε_a and various values of r_E and R. When R is sufficiently low, one can notice the gradual way in which

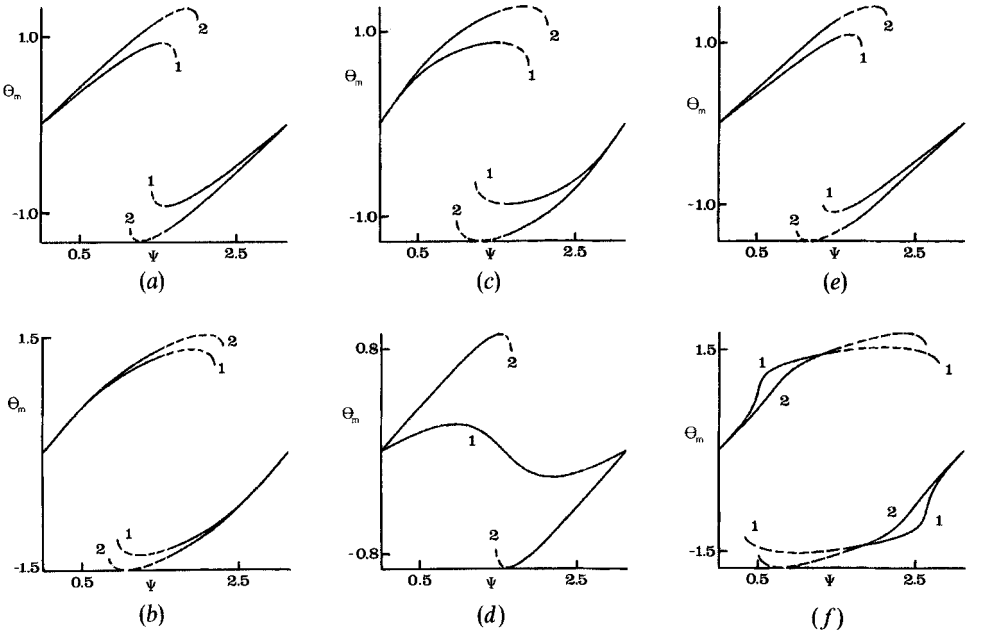

Figure 7. Effect of **E** on **H** induced bistability. Initial orientation is homeotropic along z. **E** is impressed along the sample planes. $r_E = E_x/E_B(H=0)$ from equation (4.6). $R = H/H_F(0)$ where $H_F(0)$ is the bend Freedericksz threshold from equation (3.1). $\varepsilon_\parallel$, $\varepsilon_\perp = (a)$–(c) 14·83, 12·18, (d)–(f) 18·8, 8·2. (a) $r_E = 0{\cdot}5$. $R = (1)$ 1·1, (2) 1·4. (b) $r_E = 1{\cdot}0$. $R = (1)$ 1·1, (2) 1·4. (c) $r_E = 1{\cdot}0$. $R = (1)$ 0·5, (2) 1·0. The bistability width increases with r_E for a given R. Due to the destabilizing nature of **E** which reduces the effective magnetic bend threshold bistability appears even for $R \leqq 1$. (d) $r_E = 0{\cdot}5$. $R = (1)$ 0·5, (2) 1·0. (e) $r_E = 0{\cdot}5$. $R = (1)$ 1·1, (2) 1·4. (f) $r_E = 1{\cdot}0$. $R = (1)$ 1·0, (2) 1·8. w_b increases when ε_a is enhanced for a given R and r_E. Interestingly w_b appears to diminish when R is increased at $r_E = 1{\cdot}0$ (see (f); this could be because **H** is acting on a director field which is already deformed by **E**) (see § 4.2).

the nature of the solution changes as R is enhanced. This case has been discussed in some detail in [18] (see figure 4 in § 3.4 of [18]); there it has been shown that applying first **E** and then **H** results in a deformation whose characteristics are different from one which results when **H** is impressed at a small angle with $\mathbf{n}_0$ prior to applying **E**. Another facet of the effect of **E** can be seen when R is high enough. Calculations show that an increase in R over certain ranges actually appears to diminish w_b:

$$(w_b, R) = (2{\cdot}63,\ 0{\cdot}9),\ (2{\cdot}46,\ 1{\cdot}0),\ (2{\cdot}12,\ 1{\cdot}8).$$

It must be remembered that here we are dealing with a situation where H_B does not exist due to E being high; there exists a competition between the actions of **E** (which has already produced a distortion) and **H** which is imposed on the distorted orientation; the intensity of the competition changes with ψ. When ψ is small enough, **H** has some control over the distortion; once **H** has tilted sufficiently away from $\mathbf{n}_0$ the deformation is controlled mainly by **E**. This point will be treated separately.

Another aspect worth noting is the scaling. Equation (4.4) does admit scaling but in a restricted way as compared to equation (3.2). By changing over to the variable $\xi = z/h$, Hh can be expressed in terms of R. As $E_x = V/2g$, the E_x^2 term contains the factor $\sim V^2h^2/g^2$. Hence if $h \to h\mu$, $g \to g\mu$ and $V \to V$, the E_x term in equation (4.4) will also get scaled. This is, of course, valid only for rigid anchoring. When the anchoring is weak,

even this scaling will cease to hold. It seems likely that the **H** induced bistability in the case of initial homogeneous alignment will be similarly affected by **E** applied normal to the plates.

5. Miscellaneous cases

5.1. *More complex deformation states and bistability*

In the preceding sections only distortions described by a single angle have been considered. There is no doubt that bistability may be observable in more complex deformations which are described by two angles. The elastic coupling between the two orientational degrees of freedom may give rise to novel patterns of behaviour. One of the simplest situations will arise when the nematic has $\chi_a < 0$.

In this case the Freedericksz direction for **H** is along $\mathbf{n}_0$; when **H** is normal to $\mathbf{n}_0$, no torque is exerted by **H**. Consider $\mathbf{n}_0$ homogeneously aligned along x with **H** also along x. In this configuration, **H** can couple either with a twist fluctuation to produce a twist distortion $\mathbf{n} = [\cos\phi(z), \sin(\phi(z), 0]$ above the twist threshold $H_2 = (\pi/2h)(K_2/-\mu_0\chi_a)^{1/2}$ or with the splay fluctuation to yield a splay/bend deformation $\mathbf{n} = [\cos\theta(z), 0, \sin\theta(z)]$ above the splay threshold $H_1 = (\pi/2h)(K_1/-\mu_0\chi_a)^{1/2}$. As $K_2 < K_1$, in general, the twist deformation will be favourable. Then, taking into account the sign of χ_a, the governing equation will be identical to the static limit of equation (2.19). In particular, the results of figure 5 will go over to those for a nematic with $\chi_a < 0$ if the ψ range is changed from $(0, \pi/2)$ to $(\pi/2, 3\pi/2)$; we start with **H** along y (or $-y$) and rotate **H** from the initial position in the xy plane. Even the dynamics of the twist distortion will be described by equation (2.19).

Consider now what happens when **H** is rotated in the xz plane with $H > H_2$. When **H** is along x we know that a twist distortion is produced. Suppose **H** is along z with $\mathbf{n}_0$ along x. In this position, again, **H** exerts no torque on the director field. If **H** is now rotated by a small angle towards x in the xz plane it becomes immediately clear that the deformation will involve splay/bend. Further rotation of **H** towards x should bring in twist also. Thus in this geometry the $\chi_a < 0$ nematic will suffer a distortion which will be described by two angles; this case is worth a more detailed scrutiny.

For a $\chi_a > 0$ nematic we can think of geometries in which **n** depends on two angles. A few examples will be given.

(i) Consider the twisted nematic or a long pitch cholesteric subjected to **H** normal to the plates (along the equilibrium helical axis) [37]. If H is sufficiently high, bistability can be expected when **H** is rotated about an axis parallel to the plates.

(ii) A nematic, homogeneously aligned along x, is subjected to **H** which is initially in the yz plane [38]; say. $\mathbf{H} = (0, HC_\alpha, HS_\alpha)$. Above the threshold, the distortion is described by two angles. With H sufficiently high, **H** is now rotated such that $\mathbf{H} = (HS_\beta, HC_\alpha C_\beta, HS_\alpha C_\beta)$.

(iii) Consider a non-symmetric deformation from equations (2.3) and (2.1) in the xz plane. It is obvious that when **H** is along y, there exists a threshold. In this case, with H sufficiently high, **H** is rotated in the yz plane; etc.

In all the previously mentioned geometries, the dynamics caused by a uniformly rotating **H** will involve the time rate of change of two angles. The induced shear stress will create a body force having components along two mutually perpendicular directions in the sample plane; thus the ensuing flow will be of a more general nature than the one encountered for the single angle situation. It should be interesting to study

these cases experimentally to find out how the nature of solutions will be affected. From the results of § 4 is will be clear that an additional **E** may have a non-trivial influence on the statics and dynamics in these cases also.

5.2. *Linear stability analysis*

Before concluding, it seems pertinent to attempt a linear stability analysis for at least one simple case. The aim is to determine whether the equilibrium orientation has the propensity to undergo an instability near the edges of the bistable region under the action of time dependent perturbations. As mentioned already (see § 3.1), the splay/bend geometry is somewhat complicated as the coupling between flow and orientation cannot be ignored. The twist geometry, therefore, comes to mind. The general dynamical equation (2.19) shows that as long as the twist angle is a function of z and t, there will occur no accompanying flow.

Accordingly, a perturbation $\phi''(z,t)$ is assumed to be imposed on the equilibrium twist angle $\phi(z)$ under the action of **H** from equation (2.16) with the director rigidly anchored along y at both plates. The total twist angle $\phi_T = \phi(z) + \phi''(z,t)$ obeys equation (2.19).

Substituting into equation (2.19) and linearizing with respect to ϕ'' it is found that $\phi(z)$ obeys the equilibrium equation (3.12) whose solutions have already been discussed in 3.4. The perturbation $\phi''(z,t)$ satisfies (ignoring ρ_1)

$$K_2\phi''_{,zz} - \phi''\mu_0\chi_a H^2\cos[2\psi - 2\phi(z)] - \gamma_1\dot{\phi}'' = 0 \tag{5.1}$$

and

$$\phi''(z = \pm h, t) = 0 \tag{5.2}$$

for rigid anchoring at the boundaries. The fact that the nature of the variation of ϕ'' with z and t is determined to a certain extent by $\phi(z)$ must be borne in mind. Seeking solutions of the form $\phi''(z,t) \approx \beta(z)\exp(vt)$, with v real, and changing over to $\xi = z/h$, equations (5.1) and (5.2) can be rewritten as

$$\left.\begin{aligned} &\beta_{,\xi\xi} - \beta[v(h^2\gamma_1/K_2) + (R^2\pi^2/4)\cos(2\psi - 2\phi)] = 0 \\ \text{and} \\ &\beta(\xi = \pm 1) = 0; \quad R = H/H_T, \end{aligned}\right\} \tag{5.3}$$

where H_T is the twist Freedericksz threshold. As in the case of most perturbation calculations equation (5.3) results in an eigenvalue problem. At given R and ψ, the ground state $\phi(\xi)$ is determined. Equation (5.3) is numerically solved by the orthogonal collocation method and v calculated for different ψ.

Suppose $\psi = 0$, then $\phi(\xi) = 0$ (no ground state deformation). Then,

$$\beta_{,\xi\xi} - \beta[v_0(h^2\gamma_1/K_2) + (R^2\pi^2/4)] = 0, \tag{5.4}$$

where $v_0 = v(\psi = 0)$. Putting $\beta \approx \beta_0\cos(\pi\xi/2)$, equation (5.4) reduces to $v_0 = -(\pi^2/4)(R^2 + 1)(K_2/h^2\gamma_1)$. For 5CB, $\gamma_1 = 0{\cdot}0985$ Pa s [13]. Using equation (2.22), one finds at $R = 1{\cdot}5$, $v_0 = -0{\cdot}0167\,s^{-1}$. From equation (5.3) it becomes clear that if we study the dimensionless time constant $s = vh^2\gamma_1/K_2$ instead of v, our results will become materially independent with s becoming a function of R and ψ for a given set of boundary conditions.

Figure 8 depicts the variations of s (see figure 8 (*a*)) and the free energy F (see figure 8 (*b*)) with ψ for different R. When $R < 1$ (see curve 1), figure 8 (*a*) s varies

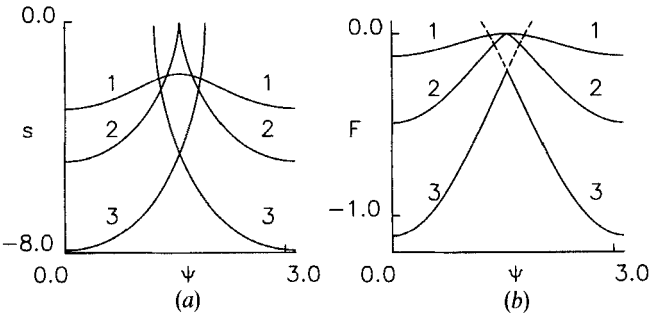

Figure 8. Plots of the dimensionless time constant $s = \nu h^2 \gamma_1 / K_2$ (of a linear perturbation) and total free energy F (of the ground state) as functions of ψ the magnetic tilt angle in twist geometry. $\mathbf{n}$ is initially aligned along γ. $\mathbf{H} = (HS_\psi, HC_\psi, 0)$ is applied in the xy plane and ψ is varied between 0 and π. At each ψ, the ground state $\mathbf{n} = (S_\phi, C_\phi, 0)$ and its free energy F are calculated using the material parameters from equation (2.22). Some typical curves of $\phi_m = \phi_m = \phi(z=0)$ have already been shown in figure 5. A linear perturbation $\phi'' \approx \beta(z)$ $\exp(\nu t)$ is imposed on $\phi(z)$; the time constants ν and s are determined with $\gamma_1 = 0{\cdot}0985$ Pa s [13]. s and F (in units of 10^{-11} J) are plotted as functions of ψ for $R = H/H_T = (1)\, 0{\cdot}5, (2)\, 1{\cdot}0$, (3) 1·5, where H_T is the twist Freedericksz threshold. The s curves are independent of the material parameters. Though the F curves are specific to the given material, their shape is material independent. The striking resemblance between the s and the F curves can be seen. It is clear that the equilibrium configuration shows a tendency to undergo instability at the edges of the bistable region (see § 5.2).

continuously with ψ but remains negative throughout the ψ range. When $R = 1$, s increases continuously from a negative value to approach zero near $\psi = \pi/2$ (see curve 2) in figure 8 (*a*). The rather sharp change in s in the middle region is possibly due to a jump in the equilibrium configuration as ψ crosses $\pi/2$. For $R > 1$ (see curves 3) the variation of s is more pronounced and $s \to 0$ at the edge of the bistability region on either branch. Interestingly, one finds a close resemblance between the shapes of the s and the F curves. Scaling analysis of equation (2.17) with $k_2 = 0$ (non-chiral nematic) shows that F for a nematic simply scales as K_2, hence the shapes of the F curves can be expected to be the same for all materials. It must be borne in mind that it is rather difficult to work close to the edge of the bistable region as $\phi(z)$ changes very rapidly there and one has to vary ψ in small increments. One can, therefore, state that the equilibrium configuration $\phi(z)$ may suffer an instability near the edges of the bistable region in twist geometry. Similar results can be expected in other cases also.

6. Conclusions

The **H** induced bistability in nematics has been studied in the limit of static deformations by considering a sequence of stable states resulting from a slow variation of the tilt of **H**. In the simple cases treated in this work, **n** is assumed to depend on only one angle. The governing equations admit scaling for rigid anchoring. For given material constants, boundary orientations and R, w_b is independent of the sample thickness. The scaling is slightly more general for twist geometry than for the splay/bend case. The scaling breaks down when the anchoring at the boundaries is weakened.

In the splay/bend geometry **H** is rotated about an axis parallel to the sample planes but normal to the plane containing **n**. When the initial orientation is uniform, w_b is found to depend on $\mathbf{n}_0$; w_b is higher for the homeotropic $\mathbf{n}_0$ than for the homogeneous $\mathbf{n}_0$ at a given R. Some of the above results are in qualitative agreement with those of

[11–13]. For given $\mathbf{n}_0$ and R, bistability can be suppressed by a sufficient diminution of the anchoring strengths at the sample planes. When the anchoring has been considerably weakened and **H** rotated sufficiently away from $\mathbf{n}_0$, a discontinuous transition may occur from a deformed state to an aligned state with **n** along **H** in all parts of the sample; this will be examined in detail separately.

The splay/bend configuration can be generalized to a rigidly anchored, non-symmetric tilt of **n** at the two boundaries. Two different cases have been studied. In one, the ground state is asymmetric while in the other it is antisymmetric. It is possible to find bistable behaviour even in these cases over certain ranges of ψ, the magnetic tilt angle. The increase of deformation in the ground state is found to be deleterious to the occurrence of bistability; it should be interesting to consider the additional effect of weak anchoring in this case.

In the twist geometry **H**, which is in the sample plane, is rotated about an axis normal to the boundaries. This case can be generalised to include the twisted and chiral nematics (the latter can have total twist $> \pi/2$ radian). Sufficient twist in the ground state is found to remove bistability for a given H. Thus these results are in qualitative accord with those for the deformed splay/bend ground state. In both the splay/bend and twist geometries bistability associated with discontinuous orientational changes can occur even in configurations where a Freedericksz threshold does not exist.

The effect of **E** impressed along the plates depends strongly on the magnitude of ε_a. It has been assumed that the nematic as well as the sample planes are insulators. When ε_a is large, **E** can produce a discontinuous transition in the bend geometry [16–18]; in the splay geometry, the stabilizing effect of **E** leads to discontinuity in the **H** induced splay transition [17]. This can be traced to the strong perturbation of **E** by director distortions.

A similar influence of **E** is found on **H** induced bistability. It should be possible, in principle, to vary the tilt of $\mathbf{n}_0$ and study the ensuing effect on **H** induced bistability. Calculations have shown [18] that in this case the effect of **E**, even in the absence of **H**, can become complex when ε_a is large. Hence, only two simple initial configurations have been chosen. For homogeneous $\mathbf{n}_0$ bistability can be suppressed, at given **H**, by increasing the stabilizing influence of **E**. The higher the ε_a the lower the E necessary to achieve this. When $\mathbf{n}_0$ is homeotropic, **E** has a destabilizing influence which reduces the effective H threshold for the bend transition. The general trend in this case is for w_b to increase with E. However, the nature of variation of distortion can be rather different depending upon whether ε_a is high or low. ε_a can be varied either by changing temperature or by using a time varying E. It may be possible to employ optical or capacitance techniques to study the way in which deformation changes for different values of ε_a.

The effect of **E** in the twist configuration has not been studied. It is, clear, however, that the influence of **E** on the **H** induced bistability may depend upon the direction along which **E** is impressed parallel to the plates. This becomes clear if we take the specific example of the rigidly anchored ground state of § 3.4 where $\mathbf{n}(z=0)$ is along y. For given E, the influence of **E** will be different for **E** along y as compared to the case when **E** is impressed at some angle, say $(\pi/4)$ radian, with the y axis.

It is straightforward to expect bistable behaviour induced by the actions of **H** and **E** in cases where **n** is described by two angles. These may be realizable in practice by varying the deformation in the ground state and by changing the tilt of the axis about which **H** is rotated. It should be interesting to study how bistability and scaling are affected in these cases.

The equations which describe bistable behaviour are merely the static limit of more general dynamical equations which account for the time rate of change of deformation caused by **H** rotating at a uniform rate. Time rate of change of **n** creates a shear stress which, in general, can result in flow. In the splay/bend geometries the occurrence of flow and the consequent coupling between flow and orientation cannot be ruled out [39]. It appears, however, that flow may be absent in the twist configuration; this might influence the time of transition in this case. The fact that bistable behaviour in the static limit can be influenced by using a deformed ground state naturally raises the question as to how this will affect the dynamics.

The total free energy F has been calculated for all distortion states. It has been found that in the region of bistability the two states, for a given tilt of **H**, have different F. It seems possible to get an order of magnitude for the time of transition from the state at one edge of the higher energy branch to the corresponding state on the lower energy branch using the free energy difference between the two branches [40]. Linear stability analysis for twist geometry shows that the equilibrium orientation has a tendency to undergo instabililty against perturbations near the edges of the bistable region. This analysis cannot give either the direction or the manner in which the deformation might change from one branch to the other. To understand the dynamics more completely it is necessary to solve the non-linear problem from equations (2.7)–(2.9) and (2.11). The direction of change is, however, intuitively obvious.

Scaling analysis shows that the time of transition between two states should get affected when the sample thickness is changed. This points towards the need to do experiments with samples of different thickness to test the scaling of bistability width and to fnd out how the time of transition (from an unstable state at one edge of the bistable region) varies with the sample thickness.

The author thanks a referee for useful comments which helped improve a previous version of the manuscript.

References

[1] Oseen, C. W., 1933, *Trans. Faraday Soc.*, **29,** 883.
[2] Frank, F. C., 1958, *Discuss. Faraday Soc.*, **25,** 19.
[3] Ericksen, J. L., 1976, *Advances in Liquid Crystals*, edited by G. H. Brown (Academic Press), p. 233.
[4] Leslie, F. M., 1979, *Advances in Liquid Crystals*, edited by G. H. Brown (Academic Press) p. 1.
[5] De Gennes, P. G., 1974, *The Physics of Liquid Crystals* (Clarendon Press).
[6] Deuling, H. J., 1978, *Solid St. Phys. Suppl.*, **4,** 77.
[7] Chandrasekhar, S., 1977, *Liquid Crystals* (Cambridge University Press).
[8] Blinov, L. M., 1983, *Electrooptical and Magnetooptical Properties of Liquid Crystals* (Wiley).
[9] Pieranski, P., Brochard, F., and Guyon, E., 1973, *J. Phys., Paris*, **34,** 35.
[10] Brochard, F., 1973, *Molec. Crystals liq. Crystals.*, **23,** 51.
[11] Onnagawa, H., and Miyashita, K., 1974, *Jap. J. appl. Phys.*, **13,** 1741.
[12] Motooka, T., and Fukuhara, A., 1979, *J. appl. Phys.*, **50,** 3322.
[13] Karn, A. J., and Shen, Y. R., 1990, *Phys. Rev.* A, **41,** 4510.
[14] Meyer, R. B., 1969, *Phys. Rev. Lett.*, **22,** 918.
[15] Dozov, I., Barbero, G., Palierne, J. F., and Durand, G., 1986, *Europhysics Lett.*, **1,** 563.
[16] Frisken, B. J., and Palffy-Muhoray, P., 1989, *Phys. Rev.* A, **39,** 1513.
[17] Frisken, B. J., and Palffy-Muhoray, P., 1989, *Phys. Rev.* A, **40,** 6099.
[18] Kini, U. D., 1990, *Liq. Crystals*, **8,** 745.
[19] Barbero, G., and Meuti, M., 1986, *J. Phys., Paris*, **47,** 341. Boyd, G. D., Cheng, J., and Ngo, P. D. T., 1980, *Appl. Phys. Lett.*, **36,** 556.

[20] RAPINI, A., and PAPOULAR, M., 1969, *J. Phys., Paris, Colloq.*, **30,** C4–54.
[21] GUYON, E., and URBACH, W., 1976, *Nonemissive Electrooptic Displays* edited by A. R. Kmetz and F. K. von Willisen (Plenum Press), p. 121.
[22] OLDANO, C., 1986, *Phys. Rev. Lett.*, **56,** 1098. MIRALDI, E., OLDANO, C., and STRIGAZZI, A., 1988, *Phys. Rev.* A, **34,** 4348.
[23] KINI, U. D., 1986, *J. Phys., Paris,* **47,** 1829.
[24] ZIMMERMANN, W., and KRAMER, L., 1986, *Phys. Rev. Lett.*, **56,** 2655.
[25] GASPAROUX, H., and PROST, J., 1971, *J. Phys., Paris,* **S2,** 65.
[26] LESLIE, F. M., LUCKHURST, G. R., and SMITH, H. J., 1972, *Chem. Phys. Lett.*, **13,** 368.
[27] BROCHARD, F., LEGER, L., and MEYER, R. B., 1975, *J. Phys., Paris Colloq.*, **36,** C1–209.
[28] HORNREICH, R. M., *Phys. Rev.* A, **15,** 1767.
[29] COHEN, G., and HORNREICH, R. M., 1990, *Phys. Rev.* A, **41,** 4402.
In general, the cholesteric equilibrium configuration is given by $\phi_{,z}=(k_2''-k_2)/K_2$ where k_2'' is some constant. Then the free energy of the equilibrium configuration $F''\approx(k_2'')^2h/K_2$. This simply amounts to saying that by fixing the cholesteric directors rigidly at the sample planes and by rotating the sample planes by different angles about the helical axis we can change the cholesteric pitch, but doing so costs energy F''. F'' is minimized when $k_2''=0$; then $\phi_{,z}=-k_2/K_2$. This is the equilibrium configuration considered in equation (2.21).
[30] FINLAYSON, B. A., 1972, *The Method of Weighted Residuals and Variational Principles* (Academic Press).
[31] TSENG, H. C., SILVER, D. L., and FINLAYSON, B. A., 1972, *Phys. Fluids,* **15,** 1213.
[32] ABRAMOWITZ, M., and STEGUN, I. A. (editor), 1972, *Handbook of Mathematical Functions* (Dover).
[33] BUNNING, J. D., FABER, T. E., and SHERRELL, P. L., 1981, *J. Phys., Paris,* **42,** 1175.
[34] LANDAU, L. D., and LIFSHITZ, E. M., 1975, *Electrodynamics of Continuous Media* (Pergamon).
[35] A comparison of equation (4.4) with equation (2.7) of [18] is instructive. In [18] the electric free energy density had been assumed to be $-D_iE_i/8\pi$; this resulted in the flexoelectric effect contributing only a surface torque and no volume terms. Thus it becomes clear that equation (4.4) will go over to equation (2.7) of [18] in the limit $e_1, e_3\to 0$. In §4 of [18] a linearized perturbation calculation has been presented to estimate the orders of magnitudes of the flexoelectric effect in the presence of weak anchoring. That estimate remains unchanged except that the flexoelectric coefficients have to be multiplied by a factor of two (for instance, equation 4.1 of [18]).
[36] As the values of $\varepsilon_{\parallel,\perp}$ at different temperatures are not available the following procedure has been adopted. It is assumed that $\varepsilon_\parallel$ and $\varepsilon_\perp$ tend to the same value $(18{\cdot}8+8{\cdot}2)/2=13{\cdot}5$ at the isotropic point. A linear variation $\varepsilon_\parallel(\Delta T)=18{\cdot}8-5{\cdot}3\ (\Delta T)$, $\varepsilon_\perp(\Delta T)=8{\cdot}2+5{\cdot}3\ (\Delta T)$ is employed such that $\varepsilon_\parallel$ and $\varepsilon_\perp=18{\cdot}8$ and $8{\cdot}2$ at $\Delta T=0$ and $\varepsilon_\parallel$ and $\varepsilon_\perp=13{\cdot}5$ at $\Delta T=1$ (isotropic point), respectively. With $\Delta T=0{\cdot}25$, $0{\cdot}5$ and $0{\cdot}75$, we get the three additional sets of $\varepsilon_\parallel$ and $\varepsilon_\perp$ used in the calculation. The elastic constant variation with temperature has been ignored.
[37] LESLIE, F. M., 1970, *Molec. Crystals liq. Crystals,* **12,** 57.
[38] DEULING, H. J., GABAY, M., GUYON, E., and PIERANSKI, P., 1975, *J. Phys., Paris,* **36,** 689.
[39] Interestingly, backflow has been neglected in [13], still good agreement has been obtained for the dynamical behaviour of the distortion. It would be instructive to find out whether flow becomes important at sufficiently high R.
[40] Let us assume that a transition can occur between two states separated by a free energy difference ΔF at the edge of the bistable region. It seems possible to write down a characteristic time purely on dimensional grounds using an average viscosity η, the sample volume and ΔF as $\tau'\approx\eta(2hA)/\Delta F$ where A is the area of the sample planes. Noting that the scaling for F should be valid for ΔF also, we find that when $h\to h\mu$, $\tau'\to\tau'\mu^2$ from equation (3.4). This means that τ' scales exactly as in equation (3.5). To get the order of magnitude of τ', the parameters of [13] are used: $(K_1, K_3)=(6{\cdot}2, 8{\cdot}8)\times 10^{-12}$ N; $\chi_a=10^{-6}$; $2h=370\ \mu$m; $\eta=0{\cdot}985$ Pa s; H $=0{\cdot}03\ T\ (R=1{\cdot}255)$; $A=10^{-4}$ m^2, in our calculations. The following results are obtained: Extremum values $\psi_e=1{\cdot}753$, $1{\cdot}389$ radian $(100{\cdot}4°, 79{\cdot}6°)$; $w_b=0{\cdot}364$ radian $(20{\cdot}8°)$; at $\psi=1{\cdot}75$, $F=0{\cdot}77\times 10^{-12}$ and $-4{\cdot}41\times 10^{-12}$ J on the two branches; $\Delta F=5{\cdot}18\times 10^{-12}$ J; hence, $\tau'=704$ s (experimental value 1800 s).